

Globular cluster star classification: application to M13

R. Caimmi*

January 24, 2022

Abstract

Starting from recent determination of Fe, O, Na abundance on a restricted sample ($N = 67$) of halo and thick disk stars, a natural and well motivated selection criterion is defined for the classification of globular cluster stars. An application is performed to M13 using a sample ($N = 112$) for which Fe, O, Na abundance has been recently inferred from observations. A comparison is made between current and earlier M13 star classification. Both O and Na empirical differential abundance distributions are determined for each class and the whole sample (with the addition of Fe in the last case) and compared with their theoretical counterparts due to cosmic scatter obeying a Gaussian distribution whose parameters are inferred from related subsamples. The occurrence of a fit between empirical and theoretical distribution is interpreted as absence of significant chemical evolution and vice versa. The procedure is repeated with regard to four additional classes according if oxygen and sodium abundance is above (stage CE) or below (stage AF) a selected threshold. Both O and Na empirical differential abundance distributions, related to the whole sample, exhibit a linear fit for AF and CE stage. Within the errors, the oxygen slope for CE stage is equal and opposite in sign with respect of the sodium slope for AF stage, while the contrary holds in dealing with the oxygen slope for AF stage with respect to the sodium

**Physics and Astronomy Department, Padua Univ., Vicolo Osservatorio 3/2, I-35122 Padova, Italy* email: roberto.caimmi@unipd.it fax: 39-049-8278212

slope for CE stage. In the light of simple models of chemical evolution applied to M13, oxygen depletion appears to be mainly turned into sodium enrichment for $[\text{O}/\text{H}] \geq -1.35$ and $[\text{Na}/\text{H}] \leq -1.45$, while one or more largely preferred channels occur for $[\text{O}/\text{H}] < -1.35$ and $[\text{Na}/\text{H}] > -1.45$. In addition, the primordial to current M13 mass ratio can be inferred from the true sodium yield in units of the sodium solar abundance. Though the above results are mainly qualitative due to large (∓ 1.5 dex) uncertainties in abundance determination, still the trend exhibited is expected to be real. The proposed classification of globular cluster stars may be extended in a twofold manner, namely to (i) elements other than Na and Fe and (ii) globular clusters other than M13.

keywords - *Galaxy: evolution* - *Galaxy: formation* - *Galaxy: halo* - *globular clusters: general* - *globular clusters: individual (M13)*.

1 Introduction

Globular clusters (GCs) are fundamental building blocks of galaxies and most of them are among the oldest stellar systems. Abundance analysis of GC stars provides valuable clues for understanding the evolution of both the cluster in itself and the hosting galaxy.

In the past, GCs were conceived as the result of an initial burst of highly efficient star formation, where the remaining gas was blown up by type II supernova (SNII) explosions together with SNII ejecta. Gas returned later from planetary nebulae was blown up by type Ia supernova (SNIa) explosions together with SNIa ejecta. Accordingly, GC stars were expected to be coeval and with element abundance affected only by cosmic scatter.

Abundance surveys with increasingly precise instrumentation disclosed consistent star-to-star abundance variation of light elements (from C to Al). At least in several cases, significant variations in He abundance were inferred. For further details and complete references, an interested reader is addressed to recent comprehensive GC abundance surveys (e.g., Carretta et al. 2009a, 2009b), reviews (e.g., Piotto 2009; Gratton et al. 2012) and investigations (e.g., Johnson and Pilachowski 2012, hereafter quoted as JP12; Conroy 2012, hereafter quoted as C12).

More specifically, interpretation of recent data disclosed the following. (i) GC normal (i.e. similar photospheric composition with respect to field halo stars) and anomalous (i.e. different photospheric composition with respect to field halo stars) stars affect the total mass to a comparable extent. (ii) Light element abundance undergoes a continuous variation passing from GC normal to most anomalous stars. (iii) GC anomalous stars exhibit enhanced

N, Na, Al; depleted O, Mg; more or less unchanged Si, Ca, Fe; enhanced He; anticorrelations such as O-Na, Mg-Al; multiple evolutionary sequences in the colour-magnitude diagram.

An explanation of the above mentioned items, within the framework of a single model, is not an easy matter. For instance, GC normal and anomalous stars in comparable proportion would imply more massive GCs at birth and/or substantially different initial stellar mass function if anomalous abundances are due to asymptotic giant branch (AGB) stars ($3 \lesssim m/m_{\odot} \lesssim 8$); a continuous variation of light elements passing from GC normal to most anomalous stars would imply (at least) two star generations separated by a time interval larger than about 0.1 Gyr and, in addition, inhomogeneous mixing between recycled material from AGB stars and inflowing primordial gas, or be a mere effect of measurement errors; O-Na and Mg-Al anticorrelations together with enhanced He would imply high-temperature proton-capture burning within AGB stars and/or rapidly rotating massive main-sequence stars and/or massive binary stars; for further details and complete references an interested reader is addressed to recent investigations (e.g., JP12; C12) and proceedings (e.g., Renzini 2013; Ventura et al. 2013).

GC anomalous stars are usually subclassified as extreme and intermediate, according if light elements are substantially or moderately enhanced/depleted with respect to field halo stars of similar Fe abundance (e.g., JP12). On the other hand, no general consensus still exists about a definition of GC normal (or primordial), intermediate and extreme stars, in absence of a related physical criterion for distinguishing one from the others. A rigorous GC star classification would be useful for tracing the past history of the Galaxy and, in fact, can be made using recent abundance determinations available for a sample of halo and low-metallicity ($[\text{Fe}/\text{H}] < -0.6$) thick disk stars (Nissen and Schuster 2010, hereafter quoted as NS10; Ramirez et al. 2012, hereafter quoted as Ra12).

The present note is aimed to this respect, where special effort is devoted to O, Na, Fe, whose abundances are known for about one hundred M13 stars (JP12). Following a current attempt (Caimmi 2013), a rigorous GC star classification is provided in Section 2. An application to M13, including both star classification and differential element abundance distribution, is shown in Section 3. The implications for halo formation and evolution, in the light of a simple model of chemical evolution, are discussed in Section 4. The conclusion is outlined in Section 5.

2 A rigorous GC star classification

The fractional logarithmic number abundance or, in short, number abundance, can be inferred from recently studied samples of solar neighbourhood FGK-type dwarf stars (NS10; Ra12), as $[Q/H]=[Q/Fe]-[Fe/H]$, for $Q = O, Na, Mg, Si, Ca, Ti, Cr, Ni, Fe$. More specifically, sample (HK) stars can be subsampled as low- α halo (LH), high- α halo (HH), thick disk (KD), GC outliers (OL). The related population is $N = 67$ (HK), 24 (LH), 25 (HH), 16 (KD), 2 (OL). Oxygen can be taken as reference element in that it is the most abundant metal and, in addition, mainly synthesised within SNII progenitors.

With regard to the $(O [O/H] [Q/H])$ plane, stars belonging to different environments display along a “main sequence”, $[Q,O] = [a_Q, b_Q, \Delta b_Q]$, bounded by two parallel straight lines:

$$[Q/H] = a_Q [O/H] + b_Q \mp \frac{1}{2} \Delta b_Q \quad ; \quad (1)$$

with the possible exception of OL stars. For further details refer to a current attempt (Caimmi 2013).

Aiming to an application to M13, where O, Na, Fe number abundances have recently been determined for about one hundred stars (JP12), the current investigation shall be restricted to $Q = Na, Fe$, keeping in mind it can be extended to any element for which number abundances are available for a large star sample. The main sequences chosen for iron and sodium, $[Fe,O] = [1.00, -0.45, 0.50]$ and $[Na,O] = [1.25, -0.40, 0.60]$, are shown in Figs. 1 and 2, respectively, top left panels, together with data from LH (squares), HH (crosses), KD (saltires), OL (“at” symbols) subsamples, taken from a current attempt (Caimmi 2013). The selected slopes are a compromise between related regression lines (Caimmi 2013).

GC stars are currently subsampled into three populations according if the O-Na anticorrelation is absent, weak, strong, defined as primordial (P), intermediate (I), extreme (E), respectively (e.g., JP12). In general, GC stars are classified as normal, if element abundance is similar to their field halo counterparts with equal iron abundance, and anomalous if otherwise (e.g., C12). In both cases, no general consensus still exists on a selection criterion.

With respect to a selected element, Q , let GC P stars be defined as those lying within the main sequence defined by field halo stars on the $(O [O/H] [Q/H])$ plane, I stars as lying within a parallel sequence towards lower $[O/H]$, E stars as lying within further parallel sequences towards lower $[O/H]$. The above mentioned selection criterion appears to be natural and well motivated, in that it relates to the main sequence defined by field halo

stars, as shown in Figs. 1 and 2, top left panels, for $Q = \text{Fe}, \text{Na}$, respectively. More specifically, the ($\text{O} [\text{O}/\text{H}] [\text{Q}/\text{H}]$) plane could be divided into an infinite number of parallel sequences, as:

$$[\text{Q}/\text{H}] = a_{\text{Q}}[\text{O}/\text{H}] + b_{\text{Q}} + \frac{2i \mp 1}{2} \Delta b_{\text{Q}} ; \quad i = 0, \mp 1, \mp 2, \dots ; \quad (2)$$

where $i = 0$ labels the main sequence populated by field halo stars, $i < 0$ and $i > 0$ label parallel sequences towards larger and lower $[\text{O}/\text{H}]$, respectively, for fixed $[\text{Q}/\text{H}]$. In this view, a generic GC star can be classified as belonging to a sequence labelled by an integer, i , with regard to a selected element, Q .

3 Application to M13

3.1 Star classification

Oxygen, sodium and iron abundance have recently been determined for a sample ($N = 113$) of red giant branch and AGB stars in M13 (JP12). Sample stars are divided therein into three classes according to the following prescriptions: $[\text{Na}/\text{Fe}] < 0.00$ - P; $[\text{O}/\text{Fe}] < 0.15$ - E; $[\text{Na}/\text{Fe}] \geq 0.00$ and/or $[\text{O}/\text{Fe}] \geq 0.15$ - I. For further details and exhaustive presentation, an interested reader is addressed to the parent paper (JP12). The following subsamples can be extracted from the parent sample: P ($N = 17$), I ($N = 70$), E ($N = 24$), where both $[\text{O}/\text{Fe}]$ and $[\text{Na}/\text{Fe}]$ are known with the exception of a (different) single star for both O and Na.

The related $[\text{Q}/\text{H}]-[\text{O}/\text{H}]$ relation, $Q = \text{Fe}, \text{Na}$, is plotted in Figs. 1, 2, respectively, top right panels, where P, I, E stars are represented as asterisks, triangles, diamonds, respectively. The main sequences, $[\text{Fe}, \text{O}] = [1.00, -0.45, 0.50]$, $[\text{Na}, \text{O}] = [1.25, -0.40, 0.60]$, are superimposed in bottom left panels of Figs. 1, 2, respectively. In addition, LH, HH, KD, OL stars (already shown in top left panels) are superimposed in bottom right panels of Figs. 1, 2, respectively.

An inspection of Fig. 1 discloses that, within the errors, P stars and a fraction of I stars lie inside the main sequence, $[\text{Fe}/\text{H}] = [\text{O}/\text{H}] - 0.45 \mp 0.25$, while the remaining I stars together with E stars display along a “horizontal branch”, $[\text{Fe}/\text{H}] = -1.6 \mp 0.2$, which also encloses the above mentioned stars belonging to the main sequence, as shown in Fig. 3. Accordingly, the following star classification can be made with respect to Fe: normal stars (class A_0) as lying within the main sequence, $[\text{Fe}, \text{O}] = [1.00, -0.45, 0.50]$; anomalous stars (class A_i) as lying within the parallel sequence, $[\text{Fe}/\text{O}] = [1.00, -0.45 + 0.50i, 0.50]$.

Let $([O/H],[Fe/H])$ be coordinates of a generic sample star on the $(O[O/H]$
 $[Fe/H])$ plane. The straight line of unit slope, passing through that point,
has intercept, $b_{Fe} = [Fe/H] - [O/H]$, and the related sequence is defined by
the inequality:

$$-0.7 + 0.5i \leq b_{Fe} < -0.2 + 0.5i \quad ; \quad (3)$$

where $i = -1, 1, 2, 3$, in the case under discussion. It is worth noticing
M13 sample stars directly shift from the main sequence, $[Fe/H] = [O/H]$
 -0.45 ∓ 0.25 , to the horizontal branch, $[Fe/H] = -1.6 \mp 0.2$, as shown in
Fig. 3.

An inspection of Fig. 2 discloses that, within the errors, a large fraction
of P stars and a few I stars lie inside the main sequence, $[Na/H] = 1.25 [O/H]$
 -0.4 ∓ 0.3 , the remaining P, I, and almost all E stars lie inside an inclined
band which defines the O-Na anticorrelation, $[Na/H] = -0.8 [O/H] - 2.5 \mp 0.7$,
and ends on a horizontal branch, $[Na/H] = -1.2 \mp 0.3$, as shown in Fig. 4.
Accordingly, the following star classification can be made with respect to Na:
normal stars (class A_0) as lying within the main sequence, $[Na,O] = [1.25,$
 $-0.40, 0.60]$; anomalous stars (class A_i) as lying within the parallel sequence,
 $[Na/O] = [1.25, -0.40 + 0.60i, 0.60]$.

Let $([O/H],[Na/H])$ be coordinates of a generic sample star on the $(O[O/H]$
 $[Na/H])$ plane. The straight line of slope, $a_{Na} = 1.25$, passing through that
point, has intercept, $b_{Na} = [Na/H] - 1.25 [O/H]$, and the related sequence is
defined by the inequality:

$$-0.7 + 0.6i \leq b_{Na} < -0.1 + 0.6i \quad ; \quad (4)$$

where $i = -1, 1, 2, 3, 4$, in the case under discussion. It is worth noticing
M13 sample stars shift from the main sequence, $[Na/H] = 1.25 [O/H]$
 -0.40 ∓ 0.30 , to the horizontal branch, $[Na/H] = -1.2 \mp 0.3$, via the parallel
sequence, $[Na/H] = 1.25 [O/H] + 0.20 \mp 0.30$, as shown in Fig. 4. The O-Na
anticorrelation, $[Na/H] = -0.8 [O/H] - 2.5 \mp 0.7$, is also plotted therein.

An inspection of Figs. 3 and 4 suggests the following classification for
M13 stars, which can be generalized to any GC where abundances have been
determined for sufficiently large star samples. Let class N (normal stars),
class T (transition stars), class H (horizontal branch stars), be defined in
terms of subclasses as:

$$N = \sum_{i=-1}^0 \sum_{j=-1}^0 (A_i, A_j) \quad ; \quad (5a)$$

$$T = \sum_{i=1}^3 (A_i, A_0) + \sum_{j=1}^4 (A_0, A_j) \quad ; \quad (5b)$$

Table 1: Partition of different M13 star populations according to the parent paper (JP12), P (primitive), I (intermediate), E (extreme), into classes with different degree of anomaly, A_i , $i = 0, \mp 1, \mp 2, \dots$, with regard to $Q = \text{Fe, Na}$, as defined in the text. Class A_{-1} is listed as $-A_1$ to save aesthetics.

pop:		P	I	E	all
Fe	Na				
$-A_1$	A_0	1	0	0	1
A_0	$-A_1$	1	0	0	1
A_0	A_0	9	2	0	11
A_0	A_1	3	25	0	28
A_0	A_2	0	5	0	5
A_1	A_0	1	0	0	1
A_1	A_1	2	7	1	10
A_1	A_2	0	30	4	34
A_1	A_3	0	1	3	4
A_2	A_2	0	0	1	1
A_2	A_3	0	0	11	11
A_2	A_4	0	0	1	1
A_3	A_4	0	0	3	3
all		17	70	24	111

$$H = \sum_{i=1}^3 \sum_{j=1}^4 (A_i, A_j) \quad ; \quad (5c)$$

where (A_i, A_j) relate to Fe and Na classification, respectively, of a selected sample star and the sum or the double sum extends over the whole set of possibilities for an assigned class. Accordingly, a selected sample star is defined by the coordinates, (A_i, A_j) , $-1 \leq i \leq 3$, $-1 \leq j \leq 4$, i and j integers, where the first and the second place within brackets relate to Fe and Na, respectively. The whole set of JP12 sample star data used in the current note is reported in Appendix A.

The partition of star classes, (A_i, A_j) , into populations, P, I, E, as defined in the parent paper (JP12), is shown in Table 1. The partition of star classes, N, T, H, as defined by Eq. (5), into populations, P, I, E, is shown in Table 2. It can be seen class N hosts about two thirds of P stars together with a few I stars, while class T hosts about one quarter of P stars and slightly less than one half of I stars. On the other hand, class H hosts a few P stars,

Table 2: Partition of different M13 star populations according to the parent paper (JP12), P (primitive), I (intermediate), E (extreme), into classes N (normal), T (transition), H (horizontal branch), as defined in the text.

pop: class	P	I	E	all
N	11	2	0	13
T	4	30	0	34
H	2	38	24	64
all	17	70	24	111

slightly more than one half of I stars and the whole amount of E stars.

In conclusion, a classification of M13 sample stars as N, T, H, instead of P, I, E, seems more complete in that it includes both O, Fe, Na, and rigorous in that it is defined in terms of mean sequences, parallel sequences, horizontal branches, O-Na anticorrelation, as shown in Figs. 3 and 4.

3.2 Differential element abundance distribution

For normalized element mass abundances, $\phi_Q = Z_Q/(Z_Q)_\odot$, the empirical differential abundance distribution reads:

$$\psi_Q = \log \frac{\Delta N}{N \Delta \phi_Q} ; \quad (6)$$

$$\Delta^\mp \psi_Q = \log \left[1 \mp \frac{(\Delta N)^{1/2}}{\Delta N} \right] ; \quad (7)$$

where ΔN is the number of sample stars binned into $[Q/H]^\mp = [Q/H] \mp \Delta[Q/H]$, N is the sample population, and the uncertainty on ΔN , $(\Delta N)^{1/2}$, has been evaluated from Poissonian errors. In addition, $\log \phi_Q = [Q/H]$ to a good extent, which implies the following:

$$\phi_Q = \frac{1}{2} \{ \exp_{10} [Q/H]^+ + \exp_{10} [Q/H]^- \} ; \quad (8)$$

$$\Delta^\mp \phi_Q = \frac{1}{2} \{ \exp_{10} [Q/H]^+ - \exp_{10} [Q/H]^- \} ; \quad (9)$$

where the bin, $\Delta \phi_Q = \Delta^+ \phi_Q + \Delta^- \phi_Q$, is variable for fixed bin, $\Delta[Q/H]$, and vice versa. For further details and complete references, an interested reader is addressed to the parent papers (Caimmi 2011a, 2012a).

The empirical differential abundance distribution, inferred from Eq. (6) with regard to JP12 sample, is listed in Table 3 for O, Na, and in Table 4 for Fe, where bins in $[Q/H]$ are centered on integer decibels and the bin width is $\Delta[Q/H] = 1$ dex. More specifically, $-2.6 \leq [O/H] \leq -0.7$; $-2.3 \leq [Na/H] \leq -0.9$; $-1.8 \leq [Fe/H] \leq -1.4$. The lower/upper uncertainty, $\Delta^\mp\psi$, and the bin semiamplitude, $\Delta^\mp\phi$, may be determined via Eqs. (7) and (9), respectively.

The results are plotted in Fig. 5 for Fe (top left panel), Na (top right panel), O (bottom right panel), all together (bottom left panel), respectively. Also plotted on each panel is the theoretical differential abundance distribution due to cosmic scatter, assumed to obey a Gaussian distribution with parameters inferred from JP12 sample, as listed in Table 5. It can be seen the empirical differential abundance distribution is consistent with its counterpart due to cosmic scatter for Fe, while the contrary holds for O and Na. The point out of scale corresponds to oxygen abundance within a single star. The theoretical differential abundance distribution due to cosmic scatter for a selected element, Q, is explicitly expressed in Appendix B.

Further inspection of Fig. 5 shows the empirical differential abundance distribution looks quite similar for O and Na in the sense that, above and below a threshold, $\phi_O \lesssim 0.045$ or $[O/H] \leq -1.35$ (class O₋) and $\phi_{Na} \lesssim 0.037$ or $[Na/H] \leq -1.45$ (class Na₋), respectively, (i) the trend suddenly changes and (ii) a linear fit to the data may safely be performed. Interestingly, N stars exhibit $[O/H] > -1.35$ for 12/13 of the total and $[Na/H] < -1.45$ for 11/13 of the total. Conversely, H stars exhibit $[O/H] \leq -1.35$ but $[Na/H] > -1.45$ (class Na₊) holds for 55/64 of the total. Finally, T stars exhibit $[O/H] > -1.35$ (class O₊) and $[Na/H] < -1.45$ for 20/34 and 11/34 of the total, respectively. The whole set of results is listed in Table 6.

The upper tail of oxygen distribution, $-0.9 \leq [O/H] \leq -0.7$, consists of one star per bin, for a total of two, placed on the lower boundary of the main sequence, [Fe,O], plotted in Fig. 3, which might be outliers. The lower tail of oxygen distribution, $-2.6 \leq [O/H] \leq -2.2$, consists of no, one, or at most two stars per bin, for a total of five, placed on the extreme left of the horizontal branch plotted in Fig. 3, which might be outliers.

The empirical differential abundance distribution, deduced from the JP12 sample for stars belonging to class N, T, H, T + H, is listed in Tables 7 and 8 for O and Na, respectively, where bin width and uncertainties are taken as in Table 3. The results are plotted in Figs. 6 and 7 for O (left panels) and Na (right panels). Also plotted on each panel is the theoretical differential abundance distribution due to the cosmic scatter, assumed to obey a Gaussian distribution, with parameters inferred from the JP12 sample as listed in Table 5. It can be seen the empirical differential abundance

Table 3: M13 empirical, differential oxygen and sodium abundance distribution deduced from the JP12 sample ($N = 112$). The error on the generic bin height has been estimated from the Poissonian error. The bin width in $[Q/H] = \log \phi_Q$ is $\Delta[Q/H] = 1$ dex. See text for further details.

ϕ	O		Na	
	ψ	ΔN	ψ	ΔN
2.528552D-03	+1.187607D+00	01		
3.183258D-03	+1.388637D+00	02		
4.007485D-03		00		
5.045125D-03	+8.876073D-01	01	+8.876073D-01	01
6.351436D-03	+7.876073D-01	01		00
7.995984D-03	+9.886373D-01	02		00
1.006635D-02	+1.189667D+00	04	+8.886373D-01	02
1.267278D-02	+1.265759D+00	06	+4.876073D-01	01
1.595408D-02	+1.232705D+00	07	+1.086577D+00	05
2.008500D-02	+1.241850D+00	09	+9.865773D-01	05
2.528552D-02	+1.266789D+00	12	+1.032705D+00	07
3.183258D-02	+1.166789D+00	12	+1.166789D+00	12
4.007485D-02	+1.266361D+00	19	+1.288637D+00	20
5.045125D-02	+1.142880D+00	18	+1.091727D+00	16
6.351436D-02	+6.906973D-01	08	+1.018056D+00	17
7.995984D-02	+2.896673D-01	04	+8.636986D-01	15
1.006635D-01	+1.896673D-01	04	+4.327053D-01	07
1.267278D-01	-5.123927D-01	01	-8.966729D-02	04
1.595408D-01		00		
2.008500D-01	-7.123927D-01	01		

Table 4: M13 empirical, differential iron abundance distribution deduced from the JP12 sample ($N = 113$). The error on the generic bin height has been estimated from the Poissonian error. The bin width in $[\text{Fe}/\text{H}] = \log \phi_{\text{Fe}}$ is $\Delta[\text{Fe}/\text{H}] = 1$ dex. See text for further details.

ϕ	ψ	ΔN
1.595408D-02	+3.837469D-01	01
2.008500D-02	+1.237989D+00	09
2.528552D-02	+1.996660D+00	65
3.183258D-02	+1.560868D+00	30
4.007485D-02	+8.868369D-01	08

Table 5: Star number, N , mean abundance, $\overline{[\text{Q}/\text{H}]} = \langle [\text{Q}/\text{H}] \rangle$, rms error, $\sigma_{[\text{Q}/\text{H}]}$, $\text{Q} = \text{O}, \text{Na}, \text{Fe}$, inferred from the JP12 sample for star classes defined above and below in the text.

class	N	$\overline{[\text{O}/\text{H}]}$	$\sigma_{[\text{O}/\text{H}]}$	$\overline{[\text{Na}/\text{H}]}$	$\sigma_{[\text{Na}/\text{H}]}$	$\overline{[\text{Fe}/\text{H}]}$	$\sigma_{[\text{Fe}/\text{H}]}$
N	13	-1.10	0.19	-1.77	0.25	-1.59	0.07
T	34	-1.30	0.10	-1.37	0.20	-1.60	0.06
H	64	-1.71	0.27	-1.26	0.19	-1.56	0.07
T+H	98	-1.57	0.30	-1.30	0.20	-1.57	0.07
N+T+H	111	-1.51	0.33	-1.35	0.26	-1.57	0.07
O ₋	76	-1.59	0.28				
O ₊	36	-1.24	0.15				
Na ₋	33			-1.66	0.19		
Na ₊	79			-1.22	0.12		

Table 6: Partition of different M13 star classes, N (normal), T (transition), H (horizontal branch), into classes, O₋, O₊, Na₋, Na₊, as defined in the text.

	O ₋	O ₊	Na ₋	Na ₊	all
N	1	12	11	2	13
T	14	20	11	23	34
H	64	0	9	55	64
all	79	32	31	80	111

distribution is consistent with its counterpart due to cosmic scatter, to an acceptable extent, for class N (O, Na), T (Na), H (Na), while the contrary holds for class T (O), H (O), T + H (O, Na).

The empirical differential abundance distribution, deduced from the JP12 sample for classes O₋, O₊, and Na₋, Na₊, is listed in Table 9 left and right panels, respectively, where bin widths and uncertainties are taken as in Table 3. The results are plotted in Fig. 8 together with related theoretical differential abundance distributions due to cosmic scatter, assumed to obey a Gaussian distribution, with parameters inferred from the JP12 sample as listed in Table 5. It can be seen the empirical differential abundance distribution is not consistent with its counterpart due to cosmic scatter.

The empirical differential oxygen and sodium abundance distribution, plotted in Fig. 5, is characterized by the presence of two stages exhibiting a nearly linear trend, which shall be named as AF, CE, for increasing element abundance. Linear fits to each stage, $\psi = a\phi + b$, are performed using the bisector regression (Isobe et al. 1990; Caimmi 2011b, 2012b), leaving aside bins related to single stars. The regression line slope and intercept estimators and related dispersion estimators are listed in Table 10 for each stage of the O and Na empirical distributions plotted in Fig. 5.

Interesting features shown in Table 10 read (i) the slope of oxygen distribution above the threshold (CE) and sodium distribution below the threshold (AF) are equal and opposite within the errors and (ii) the intercept of oxygen and sodium distribution above the threshold (CE) are equal within the errors. The regression lines are represented in Fig. 9 for each stage, according to slope and intercept values listed in Table 10. To ensure continuity, AF and CE stages are bounded by the intersections of related regression lines. The results are listed in Table 11, where OO denotes element abundance ranges without data, $0 \leq \phi \leq \phi_i$ or $\phi \geq \phi_f$, and ϕ_i and ϕ_f are the mini-

Table 7: M13 empirical, differential oxygen abundance distribution deduced from the JP12 sample for stars belonging to class N ($N = 13$), T ($N = 34$), H ($N = 64$), T + H ($N = 98$). Errors as in Table 3 and $\delta = \Delta N$ to save space. See text for further details.

ϕ	class N		class T		class H		class T + H	
	ψ	δ	ψ	δ	ψ	δ	ψ	δ
2.53D-3					+1.43D+0	1	+1.25D+0	1
3.18D-3					+1.63D+0	2	+1.45D+0	2
4.01D-3						0		0
5.05D-3					+1.13D+0	1	+9.46D-1	1
6.35D-3					+1.03D+0	1	+8.46D-1	1
8.00D-3					+1.23D+0	2	+1.05D+0	2
1.01D-2					+1.43D+0	4	+1.25D+0	4
1.27D-2					+1.51D+0	6	+1.32D+0	6
1.60D-2					+1.48D+0	7	+1.29D+0	7
2.01D-2					+1.48D+0	9	+1.30D+0	9
2.53D-2					+1.51D+0	12	+1.32D+0	12
3.18D-2					+1.41D+0	12	+1.22D+0	12
4.01D-2	+9.23D-1	1	+1.41D+0	8	+1.08D+0	7	+1.22D+0	15
5.05D-2	+1.12D+0	2	+1.64D+0	17			+1.18D+0	17
6.35D-2	+1.20D+0	3	+1.00D+0	5			+5.45D-1	5
8.00D-2	+1.10D+0	3	+6.82D-1	3			+2.23D-1	3
1.01D-1	+8.24D-1	2	+1.05D-1	1			-3.54D-1	1
1.27D-1	-4.23D-1	1						
1.60D-1		0						
2.01D-1	-2.23D-1	1						
total		13		34		64		98

Table 8: M13 empirical, differential sodium abundance distribution deduced from the JP12 sample for stars belonging to class N ($N = 13$), T ($N = 34$), H ($N = 64$) and T+H ($N = 98$). Errors as in Table 3 and $\delta = \Delta N$ to save space. See text for further details.

ϕ	class N		class T		class H		class T + H	
	ψ	δ	ψ	δ	ψ	δ	ψ	δ
5.05D-3	+1.82D+0	1						
6.35D-3		0						
8.00D-3		0						
1.01D-2	+1.82D+0	2						
1.27D-2		0	+1.01D+0	1			+5.46D-01	1
1.60D-2	+2.02D+0	5		0				0
2.01D-2	+1.52D+0	2	+8.05D-1	1	+8.32D-1	2	+8.23D-01	3
2.53D-2	+1.12D+0	1	+1.40D+0	5	+4.31D-1	1	+1.02D+00	6
3.18D-2		0	+1.30D+0	5	+1.18D+0	7	+1.22D+00	12
4.01D-2	+9.23D-1	1	+1.28D+0	6	+1.34D+0	13	+1.32D+00	19
5.05D-2	+8.23D-1	1	+1.10D+0	5	+1.13D+0	10	+1.12D+00	15
6.35D-2			+1.08D+0	6	+1.07D+0	11	+1.08D+00	17
8.00D-2			+6.82D-1	3	+9.72D-1	11	+8.92D-01	14
1.01D-1			+4.06D-1	2	+5.30D-1	5	+4.91D-01	7
1.27D-1					+3.33D-1	4	+1.48D-01	4
total		13		34		64		98

Table 9: M13 empirical, differential oxygen and sodium abundance distribution deduced from the JP12 sample for stars belonging to class O₋ ($N = 36$), $[\text{O}/\text{H}] \leq -1.35$ or $\phi \lesssim 0.040$, O₊ ($N = 76$), $[\text{O}/\text{H}] > -1.35$ or $\phi \gtrsim 0.040$, Na₋ ($N = 33$), $[\text{Na}/\text{H}] \leq -1.45$ or $\phi \lesssim 0.035$, Na₊ ($N = 79$), $[\text{Na}/\text{H}] > -1.35$ or $\phi \gtrsim 0.035$. Errors as in Table 3. See text for further details.

ϕ	O		Na	
	ψ	ΔN	ψ	ΔN
2.528552D-03	+1.356012D+00	01		
3.183258D-03	+1.557042D+00	02		
4.007485D-03		00		
5.045125D-03	+1.056012D+00	01	+1.418311D+00	01
6.351436D-03	+9.560117D-01	01		00
7.995984D-03	+1.157042D+00	02		00
1.006635D-02	+1.358072D+00	04	+1.419341D+00	02
1.267278D-02	+1.434163D+00	06	+1.018311D+00	01
1.595408D-02	+1.401110D+00	07	+1.617281D+00	05
2.008500D-02	+1.410254D+00	09	+1.517281D+00	05
2.528552D-02	+1.435193D+00	12	+1.563409D+00	07
3.183258D-02	+1.335193D+00	12	+1.697493D+00	12
4.007485D-02	+1.434765D+00	19	+1.440228D+00	20
5.045125D-02	+1.635795D+00	18	+1.243318D+00	16
6.351436D-02	+1.183613D+00	08	+1.169647D+00	17
7.995984D-02	+7.825828D-01	04	+1.015289D+00	15
1.006635D-01	+6.825828D-01	04	+5.842963D-01	07
1.267278D-01	-1.947718D-02	01	+2.412582D-01	04
1.595408D-01		00		
2.008500D-01	-2.194772D-01	01		

Table 10: Regression line slope and intercept estimators, \hat{a} and \hat{b} , and related dispersion estimators, $\hat{\sigma}_{\hat{a}}$, and $\hat{\sigma}_{\hat{b}}$, for regression models applied to the empirical differential oxygen and sodium abundance distribution plotted in Fig. 5, bottom and top right panels, respectively. The method has dealt with each stage (XX) separately. Data points on the boundary between AF and CE stages are used for determining regression lines within both of them. Bins containing a single star are not considered in the regression.

XX	\hat{a}	$\hat{\sigma}_{\hat{a}}$	\hat{b}	$\hat{\sigma}_{\hat{b}}$	class
AF	-1.4520 E+0	1.6466 E+0	1.2600 E+0	5.4019 E-2	O ₋
CE	-2.0886 E+1	4.5526 E+0	2.1346 E+0	3.0319 E-1	O ₊
AF	+1.6409 E+1	4.9000 E+0	7.2001 E-1	8.3895 E-2	Na ₋
CE	-1.3443 E+1	1.1448 E+0	1.8272 E+0	7.0398 E-2	Na ₊

mum and maximum element abundance, respectively, within sample stars. Accordingly, a vertical line instead of a regression line is considered for the intersection points related to OO-AF and CE-OO transitions.

4 Discussion

The GC star classification, defined in Section 2, is rigorous and well motivated in that it relates to the main sequence defined by field halo stars, as shown in Figs. 3 and 4 in the case under consideration of M13. The validity of the proposed classification may be tested in a twofold manner, namely by extending Figs. 3 and 4 to (i) elements other than Na, Fe, and (ii) GCs other than M13. In any case, the expected trend implies part of sample stars within the above mentioned main sequence, part on a horizontal branch (Fig. 3) or, in addition, on one or more parallel sequences towards lower oxygen abundance (Fig. 4). For an assigned element, different GCs are expected to depart from the main sequence at different points, according to their primordial abundance in that element.

Caution is needed in the interpretation of quantitative results, owing to currently large abundance measurement errors for GC stars (e.g., Renzini 2013). Let the trend exhibited by element abundance remain slightly affected even if the uncertainty on single stars is high, typically ∓ 1.5 dex for M13 (JP12). Under this assumption, valuable informations can be extracted from the empirical differential element abundance distribution, as shown in

Table 11: Transition points between adjacent stages, as determined from the intersection of related regression lines, for the empirical differential oxygen and sodium abundance distribution plotted in Fig. 9, top left and right panels, respectively.

transition	ϕ	ψ	Q
OO-AF	2.5286 E-3	+1.2563 E-0	O
AF-CE	4.5002 E-2	+1.1947 E-0	O
CE-OO	2.5286 E-1	-3.1465 E-0	O
OO-AF	4.4668 E-3	+7.9296 E-1	Na
AF-CE	3.7088 E-2	+1.3286 E-0	Na
CE-OO	1.4125 E-1	-7.1773 E-2	Na

Fig. 9 for M13, where a threshold is clearly exhibited at $[\text{O}/\text{H}] \approx -1.35$ and $[\text{Na}/\text{H}] \approx -1.45$, respectively. More specifically, different slopes in different regions could reflect the occurrence of different physical processes during the evolution.

An inspection of Table 6 shows the whole amount of H stars is depleted in oxygen, $[\text{O}/\text{H}] \leq -1.35$ (class O_-), while 55/64 of the total are enriched in sodium, $[\text{Na}/\text{H}] > -1.45$ (class Na_+), which might be interpreted in a twofold manner: either sodium enrichment is not the sole channel of oxygen depletion, or sodium is, in turn, partially depleted. In fact, the empirical differential sodium abundance distribution for classes N, T, H, is consistent, to an acceptable extent, with its theoretical counterpart due to intrinsic scatter, leaving aside a few sodium-deficient stars, as plotted in Fig. 6. With regard to oxygen, a similar trend is exhibited for class N, while the contrary holds for class T, H. The above results are consistent with little or no chemical evolution for oxygen within class N and sodium within class N, T, H. On the other hand, oxygen chemical evolution did take place, even if partially, within class T, H, and, in any case, passing from O_+ to O_- class and from Na_- to Na_+ class.

To this respect, the simplest assumption is a constant yield for both oxygen and sodium, in the light of simple MCBR (multistage closed box + reservoir) models of chemical evolution (Caimmi 2011a, 2012a) where gas inflow and outflow are allowed. In the special case of a linear fit to the empirical differential abundance distribution:

$$\psi_{\text{Q}} = a_{\text{Q}}\phi_{\text{Q}} + b_{\text{Q}} \quad ; \quad (10)$$

the slope has the explicit expression:

$$a_Q = -\frac{1}{\ln 10} \frac{(Z_Q)_\odot}{\hat{p}_Q} (1 + \kappa) ; \quad (11)$$

where $Q = O, Na$, and κ is the flow parameter, positive for outflow and negative for inflow. For further details refer to the parent papers (Caimmi 2011a, 2012a).

The oxygen-to-sodium yield ratio, inferred from Eq. (11), reads:

$$\frac{\hat{p}_O}{\hat{p}_{Na}} = \frac{a_{Na}}{a_O} \frac{(Z_O)_\odot}{(Z_{Na})_\odot} ; \quad (12)$$

where the slope ratio, a_{Na}/a_O , has necessarily to be negative for O depletion and Na enrichment, which implies an opposite sign for slopes related to classes O_-, Na_+ , and O_+, Na_- , listed in Table 10. Accordingly, the slope related to class O_- , within the errors, restricts to $0 < a_O \leq 0.1946$. Then $a_{Na}/a_O = -1$ for stars belonging to classes O_+ and Na_- , within the errors, while $a_{Na}/a_O \lesssim -69$ for stars belonging to classes O_- and Na_+ .

The substitution of the above mentioned values into Eq. (12) yields:

$$\frac{\hat{p}_O}{\hat{p}_{Na}} = -\frac{(Z_O)_\odot}{(Z_{Na})_\odot} ; \quad (13)$$

in the former alternative and

$$\frac{\hat{p}_O}{\hat{p}_{Na}} \lesssim -69 \frac{(Z_O)_\odot}{(Z_{Na})_\odot} ; \quad (14)$$

in the latter alternative. According to Eq. (13), O depletion can be entirely turned into Na enrichment during the early evolution ($[O/H] \geq -1.35$, $[Na/H] \leq -1.45$). Conversely, according to Eq. (14), O depletion appears to be mainly turned into Q other than Na enrichment during the late evolution ($[O/H] < -1.35$, $[Na/H] > -1.45$).

As an exercise, let sodium chemical evolution in M13 be considered within the framework of simple MCBR models in the linear limit (Caimmi 2011a, 2012a). Sodium may be conceived as a primary element provided it is mainly synthesised from oxygen which is, in turn, a primary element. Accordingly, the following relations hold together with Eqs. (10)-(12):

$$\frac{\mu_f}{\mu_i} = \exp_{10} \{a_Q [(\phi_Q)_f - (\phi_Q)_i]\} ; \quad (15)$$

$$s_f - s_i = \frac{(Z_Q)_\odot}{\hat{p}_Q} \mu_i [(\phi_Q)_f - (\phi_Q)_i] ; \quad (16)$$

$$D_f - D_i = \kappa (s_f - s_i) ; \quad (17)$$

$$\zeta_Q = 1 - \frac{A_Q \hat{p}_Q}{\kappa} ; \quad (18)$$

Table 12: Values of the cut parameter, ζ_{Na} , the flow parameter, κ , the active gas mass fraction, μ_f , the long-lived star mass fraction, s_f , the flowing gas mass fraction, D_f , for different values of the true sodium yield in solar sodium abundance units, $\hat{p}_{\text{Na}}/(Z_{\text{Na}})_{\odot}$, in the linear limit. For each case, upper lines correspond to Na₋ class ($[\text{Na}/\text{H}] \leq -1.45$; AF stage) and lower lines to Na₊ class ($[\text{Na}/\text{H}] > -1.45$; CE stage). To save space, \hat{p}_{Na} stands for $\hat{p}_{\text{Na}}/(Z_{\text{Na}})_{\odot}$, XX denotes the stage and cls the class. For further details refer to the text.

\hat{p}_{Na}	ζ_{Na}	κ	μ_f	s_f	D_f	XX	cls
0.5	1.0003E-0	-1.9893E+1	3.4302E-0	1.2863E-1	-2.5588E-0	AF	Na ₋
	9.9960E-1	+1.4477E+1	1.3648E-1	3.4144E-1	+5.2208E-1	CE	Na ₊
1.0	1.0003E-0	-3.8786E+1	3.4302E-0	6.4315E-2	-2.4945E-0	AF	Na ₋
	9.9961E-1	+2.9954E+1	1.3648E-1	1.7072E-1	+6.9280E-1	CE	Na ₊
2.0	1.0003E-0	-7.6571E+1	3.4302E-0	3.2157E-2	-2.4623E-0	AF	Na ₋
	9.9962E-1	+6.0907E+1	1.3648E-1	8.5361E-2	+7.7816E-1	CE	Na ₊

where μ is the gas mass fraction, s the long-lived star mass fraction, D the flowing gas mass fraction, ζ the ratio of Q abundance within the flowing gas to Q abundance within the pre existing gas, A_{Q} a coefficient which may safely be expressed as $A_{\text{Q}} = 2(Z_{\text{O}})_{\odot}/(Z_{\text{Q}})_{\odot}$, $\text{Q} = \text{Na}$ in the case under discussion and the indexes, i, f, denote initial and final values, respectively, with regard to the stage considered. The free parameter is chosen to be the true sodium yield, \hat{p}_{Na} .

The cut parameter, ζ_{Na} , the flow parameter, κ , the active (i.e. available for star formation) gas mass fraction, μ_f , the long-lived star mass fraction, s_f , the flowing gas mass fraction, D_f , determined in the linear limit for a true sodium yield in solar sodium abundance units, $\hat{p}_{\text{Na}}/(Z_{\text{Na}})_{\odot} = 0.5, 1.0, 2.0$, are listed in Table 12. The parameters, κ , D_f , are negative for inflow and positive for outflow, respectively. For each case, upper lines correspond to Na₋ class ($[\text{Na}/\text{H}] \leq -1.45$; AF stage) and lower lines to Na₊ class ($[\text{Na}/\text{H}] > -1.45$; CE stage).

Solar abundances are inferred from recent data (Asplund et al. 2009) as $(Z_{\text{Na}})_{\odot} = 2.950 \cdot 10^{-5}$ and $(Z_{\text{O}})_{\odot} = 5.786 \cdot 10^{-3}$ (Caimmi 2013). The initial values at the AF stage are chosen as $\mu_i = 1$; $s_i = 0$; $D_i = 0$; accordingly, μ_f is independent of $\hat{p}_{\text{Na}}/(Z_{\text{Na}})_{\odot}$ via Eq. (15) and the ratio, $(s_f)_{\text{CE}}/(s_f)_{\text{AF}}$, is

independent of $\hat{p}_{\text{Na}}/(Z_{\text{Na}})_{\odot}$ via Eq. (16). If $(s_f)_{\text{CE}}$ and $(\mu_f)_{\text{AF}} + (s_f)_{\text{AF}}$ relate to the current and the primordial M13 mass, respectively, an inspection of Table 12 shows the primordial to current mass ratio amounts to about 10, 20, 40, for $\hat{p}_{\text{Na}}/(Z_{\text{Na}})_{\odot} = 0.5, 1.0, 2.0$, respectively, according to Eqs. (15)-(16). Then the M13 primordial mass can be inferred, in the framework of the model, from the knowledge of the true sodium yield.

5 Conclusion

The main results of the current paper may be summarized as follows.

- (1) Basing on the “mean sequence” defined by halo and thick disk low-metallicity ($[\text{Fe}/\text{H}] < -0.6$) stars on the ($\text{O}[\text{O}/\text{H}][\text{Q}/\text{H}]$) plane (Caimmi 2013), a natural and well motivated selection criterion has been defined for classifying GC stars with respect to a selected element, Q, and to oxygen, O.
- (2) An application has been performed to M13 using a star sample ($N = 112$) for which O, Na, Fe abundance is available (JP12): previously classified primordial stars are found to lie (leaving aside two exceptions) within the above mentioned main sequence (class N); previously classified intermediate stars are found to lie (in comparable amount) within both a parallel main sequence (towards lower $[\text{O}/\text{H}]$; class T) and a “horizontal branch” (class H); previously classified extreme stars are found to lie within the above mentioned horizontal branch; as shown in Table 2 and in Figs. 3, 4.
- (3) Both O and Na empirical differential abundance distributions have been determined for each class and the whole sample (with the addition of Fe in the last case) and compared with their theoretical counterparts due to cosmic scatter obeying a Gaussian distribution whose parameters were inferred from related subsamples. For the whole sample, an acceptable fit has been found only for Fe, as shown in Fig. 5, which has been extended to class N for both O and Na and to class T and H for Na with the exception of a few sodium-deficient stars, as shown in Fig. 6. No fit occurs for both T + H class and for stars where $[\text{O}/\text{H}] < -1.35$ (class O_-), $[\text{O}/\text{H}] \geq -1.35$ (class O_+), $[\text{Na}/\text{H}] \leq -1.45$ (class Na_-), $[\text{Na}/\text{H}] > -1.45$ (class Na_+), as shown in Figs. 7, 8, which has been interpreted as a signature of chemical evolution.
- (4) Both empirical O and Na differential abundance distributions, related to the whole sample, have been fitted by a straight line with regard

to O_- , O_+ , Na_- , Na_+ class, respectively, where the slopes related to O_+ and Na_- class were equal and opposite in sign within the errors, while the contrary was found for O_- and Na_+ class, as shown in Table 10 and in Fig. 9. The above results have been interpreted as consistent with oxygen depletion mainly turned into sodium enrichment for $[O/H] \geq -1.35$, $[Na/H] \leq -1.45$, and implying oxygen depletion through most preferred channels with respect to Na for $[O/H] < -1.35$, $[Na/H] > -1.45$.

- (5) In the light of simple MCBR models of chemical evolution in the linear limit, the ratio of M13 primordial to current mass has been found to be proportional to the true sodium yield in units of sodium solar abundance, as shown in Table 12, where $M_{\text{primordial}}/M_{\text{current}} = [(\mu_f)_{\text{AF}} + (s_f)_{\text{AF}}]/(s_f)_{\text{CE}}$.

As current abundance determinations, $[Q/H]$, are affected by large (∓ 1.5 dex) uncertainties in GC stars, the above results are to be conceived as mainly qualitative, but the trends shown are expected to be real. As already mentioned in Section 4, the validity of the proposed classification may be tested in a twofold manner, namely by extending Figs. 3 and 4 to (i) elements other than Na, Fe, and (ii) GCs other than M13.

References

- [1] Asplund, M., Grevesse, N., Sauval, A.J., Scott, P.: 2009, *Ann. Rev. Astron. Astrophys.*, 47, 481.
- [2] Caimmi, R.: 2011a, *Ser. Astron. J.* 183, 37.
- [3] Caimmi, R.: 2011b, *New Astron.*, 16, 337.
- [4] Caimmi, R.: 2012a, *Ser. Astron. J.* 185, 35.
- [5] Caimmi, R.: 2012b, *Intellectual Archive* 1, 71, ISSN 1929-4700 Toronto (arxiv 1111.2680).
- [6] Caimmi, R.: 2013, in preparation. (arxiv 1306.6750).
- [7] Carretta, E., Bragaglia, A., Gratton, R., Lucatello, S. 2009a, *A&A*, 505, 139
- [8] Carretta, E., Bragaglia, A., Gratton, R. G., et al. 2009b, *A&A*, 505, 117
- [9] Conroy, C., 2012, *ApJ* 758, 21. (C12)

- [10] Gratton, R. G., Carretta, E., Bragaglia, A. 2012, *A&AR*, 20, 50
- [11] Isobe, T., Feigelson, E.D., Akritas, M.G., Babu, G.J.: 1990, *Astrophys. J.*, 364, 104.
- [12] Johnson, C.I., Pilachowski, C.A., 2012, *ApJ L* 754, L38 (JP12)
- [13] Nissen, P. E., Schuster, W. J.: 2010, *Astron. Astrophys.*, 511, L10. (NS10)
- [14] Piotto, G. 2009, in *Proc. IAU Symposium 258*, ed. E. E. Mamajek, D. R. Soderblom, & R. F. G. Wyse (Cambridge: Cambridge Univ. Press), 233
- [15] Ramirez, I., Melendez, J., Chanamé, J. 2012, *ApJ*, 757, 164 (Ra12)
- [16] Renzini, A.: 2013, *MemSAIt* , .
- [17] Ventura, P., Di Criscienzo, M., Carini, R., D’Antona, F. 2013, *Mon. Not. R. Astron. Soc.*, in press (arxiv 1303.3912).

Appendix

A JP12 sample star data

The whole set of JP12 sample star data used in the text is listed in Tables 13-16, where the following denomination or value appears on each column: (1) star name; (2) other star name; (3) $[O/H]$; (4) $[Fe/H]$; (5) $[Na/H]$; (6) b_{Fe} via Eq. (1) where $a_{Fe} = 1.00$; (7) b_{Na} via Eq. (1) where $a_{Na} = 1.25$; (8) population (P, I, E) as defined in the parent paper (JP12); (9) Fe class according to Eq. (3); (10) Na class according to Eq. (4); (11) Fe-Na class (N, T, H) according to Eq. (5).

B Differential element abundance distribution due to cosmic scatter

Let a sample be made of N long-lived coeval stars belonging to the same generation, where the abundance of the primordial gas was affected from cosmic scatter. Let the related distribution be Gaussian in $[Q/H]$ with respect

Table 13: M13 star classification according to the parent paper (JP12) and the current attempt. Number abundances, $[O/H]$, $[Fe/H]$, $[Na/H]$, are taken or inferred from the parent paper. Intercepts, b_Q , relate to the straight line, $[Q/H] = a_Q[O/H] + b_Q$, passing through the point, $([Q/H], [O/H])$, where $Q = Fe, Na$, $a_{Fe} = 1.00$, $a_{Na} = 1.25$. Population P (primitive), I (intermediate), E (extreme), are defined as in the parent paper. Classes with different degree of anomaly, A_i , $i = 0, \mp 1, \mp 2, \dots$, with regard to $Q = Fe, Na$, are defined as in the text. Class A_{-1} is listed as $-A_1$ to save aesthetics. Class N (normal), T (transition), H (horizontal branch), are defined as in the text. See text for further details.

name	other	$[O/H]$	$[Fe/H]$	$[Na/H]$	b_{Fe}	b_{Na}	p	Fe	Na	c
L 324	V11	-1.96	-1.50	-1.23	0.46	1.22	E	A_2	A_3	H
L 598	...	-1.35	-1.44	-1.58	-0.09	0.11	P	A_1	A_1	H
L 629	...	-1.63	-1.57	-1.37	0.06	0.67	I	A_1	A_2	H
L 194	II-90	-1.90	-1.49	-1.13	0.41	1.25	E	A_2	A_3	H
L 973	I-48	-2.55	-1.50	-1.23	1.05	1.96	E	A_3	A_4	H
L 835	V15	-2.16	-1.50	-1.10	0.66	1.60	E	A_2	A_3	H
L 954	IV-25	-2.00	-1.48	-1.12	0.52	1.38	E	A_2	A_3	H
L 940	...	-2.09	-1.53	-1.36	0.56	1.25	E	A_2	A_3	H
L 70	II-67	-2.45	-1.45	-1.12	1.00	1.94	E	A_3	A_4	H
L 199	III-63	-1.51	-1.61	-1.41	-0.10	0.48	I	A_1	A_1	H
L 853	...	-1.50	-1.51	-1.31	-0.01	0.57	I	A_1	A_2	H
L 261	...	-1.59	-1.59	-1.53	0.00	0.46	I	A_1	A_1	H
L 262	...	-1.52	-1.58	-1.36	-0.06	0.54	I	A_1	A_2	H
L 72	III-73	-1.45	-1.59	-1.75	-0.14	0.06	P	A_1	A_1	H
L 240	II-34	-1.82	-1.42	-1.12	0.40	1.16	E	A_2	A_3	H
L 481	...	-2.26	-1.49	-1.12	0.77	1.71	E	A_2	A_4	H
L 250	...	-1.86	-1.58	-1.20	0.28	1.12	E	A_1	A_3	H
L 384	...	-1.25	-1.61	-1.57	-0.36	-0.01	I	A_0	A_1	T
L 465	...	-1.26	-1.64	-1.79	-0.38	-0.21	P	A_0	A_0	N
L 96	II-76	-1.20	-1.63	-1.72	-0.43	-0.22	P	A_0	A_0	N
L 845	...	-2.05	-1.57	-1.17	0.48	1.39	E	A_2	A_3	H
L 745	I-13	-1.35	-1.55	-1.91	-0.20	-0.22	P	A_1	A_0	T
L 584	...	-1.40	-1.63	-1.95	-0.23	-0.20	I	A_0	A_0	N
L 296	...	-1.45	-1.71	-1.43	-0.26	0.38	I	A_0	A_1	T
L 367	...	-2.01	-1.57	-1.17	0.44	1.34	E	A_2	A_3	H
L 316	III-59	-1.80	-1.62	-1.38	0.18	0.87	E	A_1	A_2	H
L 549	...	-1.35	-1.62	-1.18	-0.27	0.51	I	A_0	A_2	T
L 674	...	-1.61	-1.62	-1.18	-0.01	0.83	I	A_1	A_2	H

Table 14: Continuation of Table 13.

name	other	[O/H]	[Fe/H]	[Na/H]	b_{Fe}	b_{Na}	p	Fe	Na	c
L 398	...	-1.30	-1.55	-1.47	-0.25	0.16	I	A ₀	A ₁	T
L 244	III-52	-1.70	-1.62	-1.36	0.08	0.77	I	A ₁	A ₂	H
L 252	II-33	-1.38	-1.60	-1.58	-0.22	0.15	I	A ₀	A ₁	T
L 830	...	-1.91	-1.59	-1.07	0.32	1.32	E	A ₂	A ₃	H
L 938	IV-53	-1.17	-1.63	-1.21	-0.46	0.25	P	A ₀	A ₁	T
L 158	II-57	-1.80	-1.58	-1.52	0.22	0.73	E	A ₁	A ₂	H
L 666	...	-1.30	-1.57	-1.45	-0.27	0.17	I	A ₀	A ₁	T
L 77	III-18	-1.86	-1.62	-1.18	0.24	1.14	E	A ₁	A ₃	H
L 169	III-37	-1.86	-1.52	-1.03	0.34	1.29	E	A ₂	A ₃	H
L 825	...	-1.61	-1.55	-1.12	0.06	0.89	I	A ₁	A ₂	H
L 353	II-40	-1.23	-1.58	-1.81	-0.35	-0.27	P	A ₀	A ₀	N
L 594	...	-1.45	-1.57	-1.12	-0.12	0.69	I	A ₁	A ₂	H
L 777	I-24	-1.37	-1.57	-1.43	-0.20	0.28	I	A ₁	A ₁	H
L 1073	...	-1.32	-1.64	-1.58	-0.32	0.07	I	A ₀	A ₁	T
L 754	...	-1.26	-1.60	-1.51	-0.34	0.07	I	A ₀	A ₁	T
L 198	...	-1.51	-1.53	-1.06	-0.02	0.83	I	A ₁	A ₂	H
L 687	IV-15	-1.55	-1.65	-1.52	-0.10	0.42	I	A ₁	A ₁	H
L 863	I-42	-1.70	-1.59	-1.48	0.11	0.64	I	A ₁	A ₂	H
L 1023	IV-61	-1.71	-1.50	-1.19	0.21	0.95	E	A ₁	A ₂	H
L 877	I-50	-1.45	-1.66	-1.29	-0.21	0.52	I	A ₀	A ₂	T
L 919	IV-28	-1.75	-1.62	-1.27	0.13	0.92	I	A ₁	A ₂	H
K 656	...	-1.31	-1.57	-1.54	-0.26	0.10	I	A ₀	A ₁	T
L 343	...	-1.25	-1.60	-1.41	-0.35	0.15	I	A ₀	A ₁	T
L 592	...	-1.40	-1.68	-1.37	-0.28	0.38	I	A ₀	A ₁	T
L 476	...	-1.32	-1.62	-1.40	-0.30	0.25	I	A ₀	A ₁	T
L 269	...	-1.76	-1.65	-1.44	0.11	0.76	I	A ₁	A ₂	H
L 948	IV-35	-1.39	-1.64	-1.46	-0.25	0.28	I	A ₀	A ₁	T
L 967	I-86	-2.01	-1.55	-1.17	0.46	1.34	E	A ₂	A ₃	H
L 1030	I-77	-1.30	-1.61	-1.46	-0.31	0.17	I	A ₀	A ₁	T
L 644	...	-1.66	-1.62	-1.30	0.04	0.78	I	A ₁	A ₂	H
L 773	I-23	-1.35	-1.66	-1.32	-0.31	0.37	I	A ₀	A ₁	T
L 956	...	-1.45	-1.63	-1.26	-0.18	0.55	I	A ₁	A ₂	H
K 228	J 3	-1.51	-1.45	-0.93	0.06	0.96	I	A ₁	A ₂	H
L 176	II-87	-1.40	-1.61	-1.24	-0.21	0.51	I	A ₀	A ₂	T
K 188	A1	-1.15	-1.52	-1.30	-0.37	0.14	I	A ₀	A ₁	T
L 436	...	-1.70	-1.78	-1.42	-0.08	0.70	I	A ₁	A ₂	H
L 114	III-7	-1.45	-1.61	-1.26	-0.16	0.55	I	A ₁	A ₂	H

Table 15: Continuation of Table 14.

name	other	[O/H]	[Fe/H]	[Na/H]	b_{Fe}	b_{Na}	p	Fe	Na	c
L 370	...	-1.85	-1.66	-1.39	0.19	0.92	E	A_1	A_2	H
L 1043	BAUM13	-1.43	-1.67	-1.10	-0.24	0.69	I	A_0	A_2	T
L 766	I-12	-1.65	-1.63	-1.43	0.02	0.63	I	A_1	A_2	H
L 172	III-45	-1.40	-1.58	-1.41	-0.18	0.34	I	A_1	A_1	H
L 26	J38	-1.65	-1.51	-1.23	0.14	0.83	I	A_1	A_2	H
L 168	II-28	-1.03	-1.64	-2.30	-0.61	-1.01	P	A_0	$-A_1$	N
L 193	II-94	-1.60	-1.56	-1.01	0.04	0.99	I	A_1	A_2	H
L 726	IV-19	-1.28	-1.54	-1.38	-0.26	0.22	I	A_0	A_1	T
L 793	...	-1.05	-1.59	-1.72	-0.54	-0.41	P	A_0	A_0	N
K 699	X 24	-1.38	-1.60	-1.20	-0.22	0.53	I	A_0	A_2	T
L 677	IV-4	-1.65	-1.59	-0.88	0.06	1.18	I	A_1	A_3	H
L 18	...	-1.55	-1.65	-1.54	-0.10	0.40	I	A_1	A_1	H
L 800	IV-18	-1.30	-1.59	-1.35	-0.29	0.27	I	A_0	A_1	T
L 1032	I-76	-1.40	-1.59	-1.67	-0.19	0.08	E	A_1	A_1	H
L 871	I-19	-2.46	-1.62	-0.99	0.84	2.09	E	A_3	A_4	H
L 955	IV-22	-1.45	-1.54	-1.25	-0.09	0.56	I	A_1	A_2	H
L 609	...	-1.30	-1.69	-1.22	-0.39	0.41	I	A_0	A_1	T
L 81	II-23	-1.58	-1.60	-1.04	-0.02	0.93	I	A_1	A_2	H
L 1001	I-49	-1.30	-1.54	-1.60	-0.24	0.02	P	A_0	A_1	T
K 422	...	-1.10	-1.54	-1.32	-0.44	0.05	I	A_0	A_1	T
L 1060	I-65	-1.65	-1.57	-1.36	0.08	0.70	I	A_1	A_2	H
L 162	III-43	-1.56	-1.48	-1.40	0.08	0.55	I	A_1	A_2	H
L 488	...	-1.35	-1.55	-1.30	-0.20	0.39	I	A_1	A_1	H
L 1051	IV-78	-1.86	-1.57	-1.20	0.29	1.12	E	A_1	A_3	H
L 1114	...	-1.35	-1.65	-1.64	-0.30	0.05	I	A_0	A_1	T
L 557	...	-1.13	-1.58	-1.79	-0.45	-0.38	P	A_0	A_0	N
L 79	...	-1.00	-1.55	-1.81	-0.55	-0.56	P	A_0	A_0	N
K 659	...	-1.40	-1.39	-1.06	0.01	0.69	I	A_1	A_2	H
L 140	III-25	-1.50	-1.61	-1.00	-0.11	0.88	I	A_1	A_2	H
K 674	...	-0.90	-1.59	-1.33	-0.69	-0.20	I	A_0	A_0	N
L 787	I-2	-1.28	-1.58	-1.11	-0.30	0.49	I	A_0	A_1	T
L 1050	...	-1.40	-1.47	-0.07	A_1
L 1072	IV-80	-1.45	-1.55	-0.91	-0.10	0.90	I	A_1	A_2	H
L 423	II-7	-1.00	-1.51	-1.62	-0.51	-0.37	P	A_0	A_0	N
L 824	I-39	-1.25	-1.56	-1.19	-0.31	0.37	I	A_0	A_1	T
L 1096	I-67	-1.65	-1.58	-1.25	0.07	0.81	I	A_1	A_2	H
L 1097	...	-1.80	-1.48	-1.28	0.32	0.97	E	A_2	A_2	H

Table 16: Continuation of Table 15.

name	other	[O/H]	[Fe/H]	[Na/H]	b_{Fe}	b_{Na}	p	Fe	Na	c
L 29	II-63	-1.59	-1.07
K 224	J 37	-1.15	-1.53	-1.03	-0.38	0.41	I	A_0	A_1	T
L 137	...	-1.25	-1.47	-1.07	-0.22	0.49	I	A_0	A_1	T
L 16	J50	-1.17	-1.61	-1.79	-0.44	-0.33	P	A_0	A_0	N
K 647	...	-1.65	-1.58	-1.51	0.07	0.55	I	A_1	A_2	H
L 93	III-40	-1.00	-1.42	-1.03	-0.42	0.22	I	A_0	A_1	T
L 1095	I-69	-1.30	-1.62	-1.68	-0.32	-0.05	P	A_0	A_1	T
L 6	J11	-1.70	-1.68	-1.32	0.02	0.81	I	A_1	A_2	H
L 101	II-60	-1.28	-1.68	-2.00	-0.40	-0.40	P	A_0	A_0	N
L 32	II-64	-1.43	-1.44	-0.94	-0.01	0.85	I	A_1	A_2	H
CM 12	...	-0.65	-1.39	-1.40	-0.74	-0.59	P	$-A_1$	A_0	N

to a selected element, Q, and normalized to the sample population, N . The explicit expression reads:

$$\frac{dN}{N} = \frac{1}{\sqrt{2\pi}\sigma} \exp\left(-\frac{x^2}{2\sigma^2}\right) dx ; \quad (19)$$

$$x = [\text{Q}/\text{H}] - \langle [\text{Q}/\text{H}] \rangle ; \quad (20)$$

where dN is the expected star number within a bin, centered on x , of infinitesimal width, dx .

Keeping in mind $[\text{Q}/\text{H}] = \log \phi_{\text{Q}}$ to a good extent (e.g., Caimmi 2011a), the infinitesimal bin width reads:

$$dx = d[\text{Q}/\text{H}] = \frac{1}{\ln 10} \frac{d\phi_{\text{Q}}}{\phi_{\text{Q}}} ; \quad (21)$$

which is equivalent to:

$$\frac{dx}{d\phi_{\text{Q}}} = \frac{1}{\ln 10} \frac{1}{\phi_{\text{Q}}} ; \quad (22)$$

according to Eq. (20).

The theoretical differential element abundance distribution due to cosmic scatter is inferred from the theoretical counterpart of Eq. (6):

$$\psi_{\text{Q}} = \log \frac{dN}{N d\phi_{\text{Q}}} ; \quad (23)$$

after substitution of Eqs. (19) and (22) into (23). The result is:

$$(\psi_Q)_{cs} = \log \left\{ \frac{1}{\ln 10} \frac{1}{\sqrt{2\pi}\sigma} \exp \left[-\frac{(\log \phi_Q - \overline{\log \phi_Q})^2}{2\sigma^2} \right] \frac{1}{\phi_Q} \right\} ; \quad (24)$$

where cs denotes cosmic scatter and $\overline{\log \phi_Q} = \langle [Q/H] \rangle$.

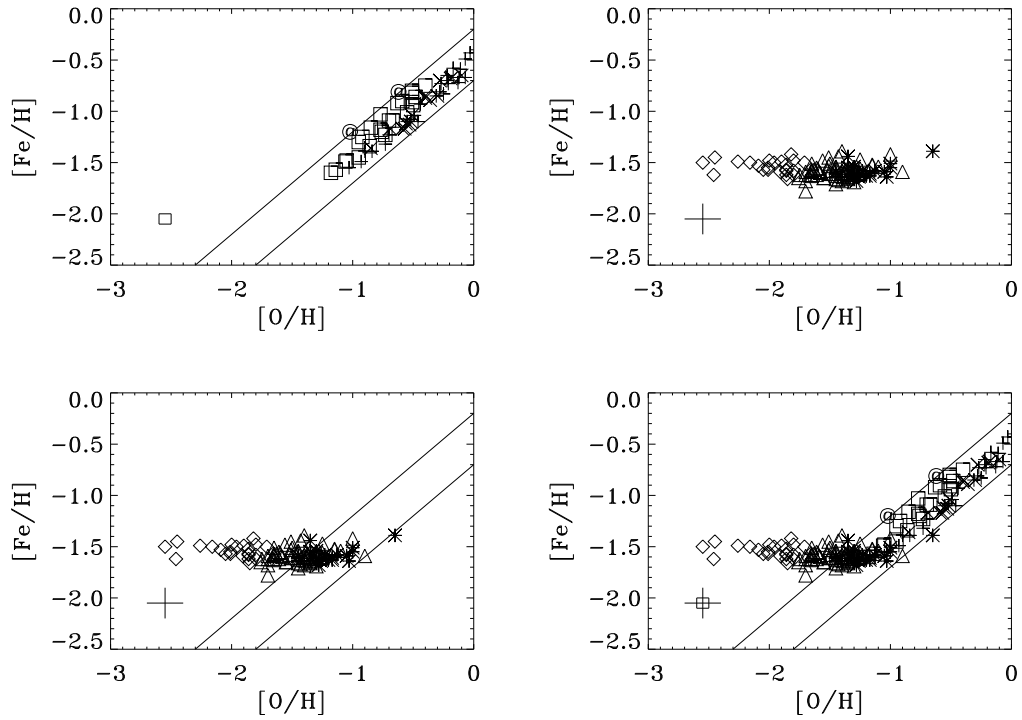


Figure 1: The selected main sequence, $[\text{Fe}/\text{H}] = [\text{O}/\text{H}] - 0.45 \pm 0.25$, together with the $[\text{Fe}/\text{H}]$ - $[\text{O}/\text{H}]$ relation for LH (squares), HH (crosses), KD (saltires), OL (“at” symbols) populations, inferred (Caimmi 2013) from recent investigations (NS10; Ra12), top left panel; the $[\text{Fe}/\text{H}]$ - $[\text{O}/\text{H}]$ relation for primordial (asterisks), intermediate (triangles), extreme (diamonds) M13 stars, inferred from recent subsampled data (JP12), top right panel; as in top right panel with the main sequence, $[\text{Fe}/\text{H}] = [\text{O}/\text{H}] - 0.45 \pm 0.25$, superimposed, bottom left panel; as in bottom left panel with LH, HH, KD, OL data superimposed, bottom right panel. Typical errors are represented as a cross (M13) and a square (LH, HH, KD, OL) when appropriate, on the bottom left of each panel. For further details refer to the text.

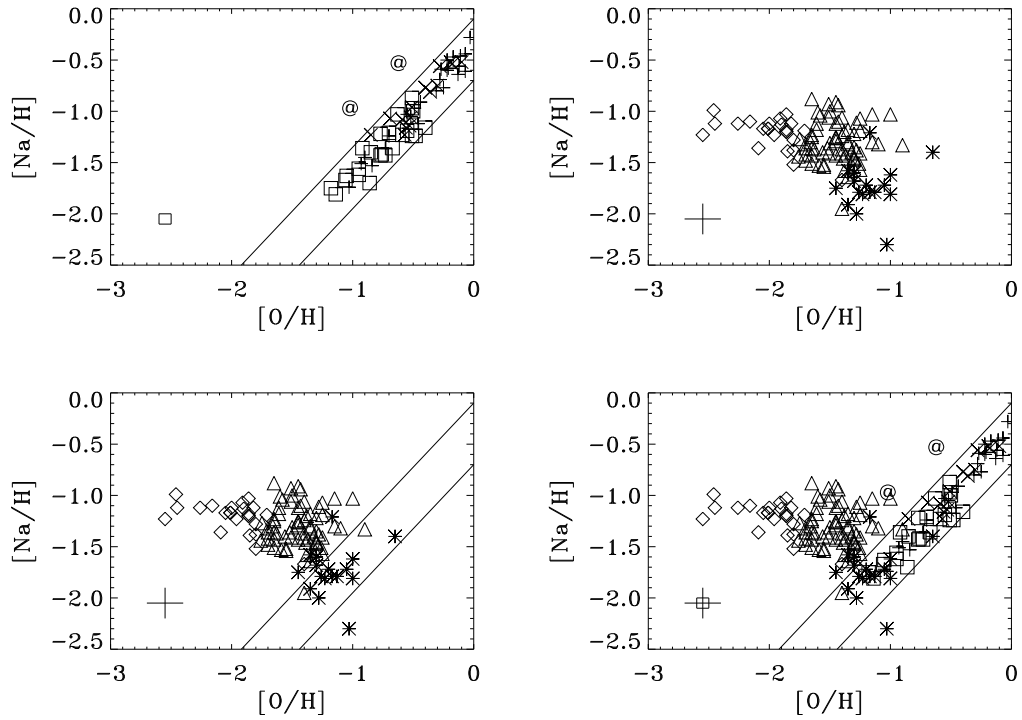


Figure 2: The selected main sequence, $[\text{Na}/\text{H}] = [\text{O}/\text{H}] - 0.4 \pm 0.3$, together with the $[\text{Na}/\text{H}]$ - $[\text{O}/\text{H}]$ relation for LH (squares), HH (crosses), KD (saltires), OL (“at” symbols) populations, inferred (Caimmi 2013) from recent investigations (NS10; Ra12), top left panel; the $[\text{Na}/\text{H}]$ - $[\text{O}/\text{H}]$ relation for primordial (asterisks), intermediate (triangles), extreme (diamonds) M13 stars, inferred from recent subsampled data (JP12), top right panel; as in top right panel with the main sequence, $[\text{Na}/\text{H}] = [\text{O}/\text{H}] - 0.4 \pm 0.3$, superimposed, bottom left panel; as in bottom left panel with LH, HH, KD, OL data superimposed, bottom right panel. Typical errors are represented as a cross (M13) and a square (LH, HH, KD, OL) when appropriate, on the bottom left of each panel. For further details refer to the text.

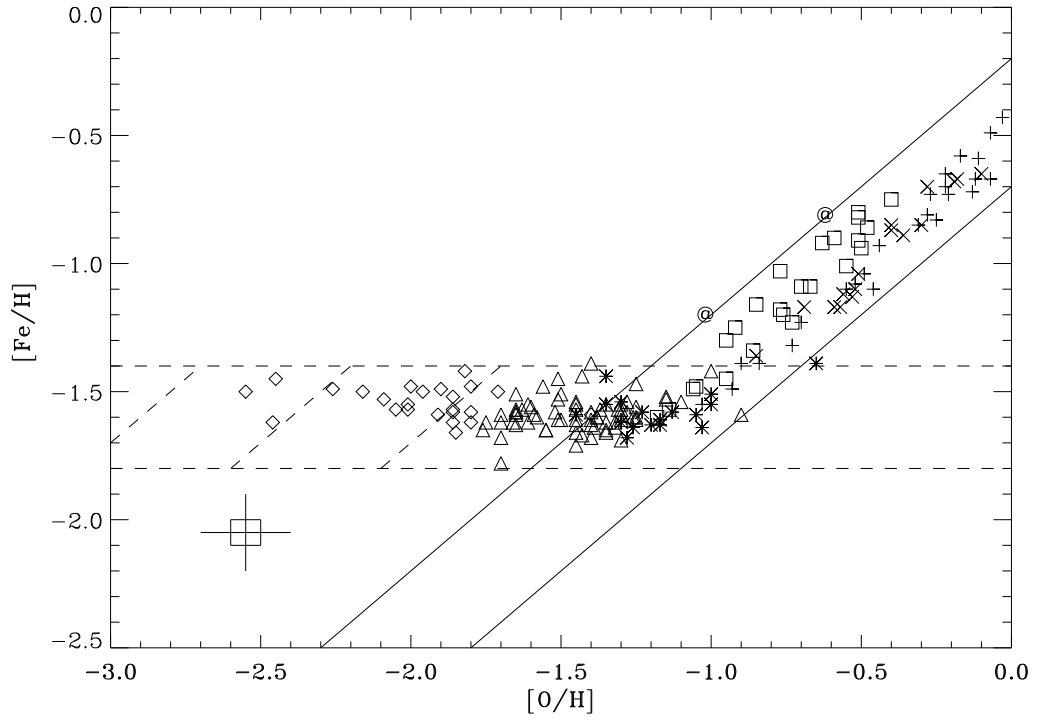


Figure 3: Zoom of Fig. 1, bottom right panel, where the parallel sequences, $[\text{Fe}/\text{H}] = [\text{O}/\text{H}] - 0.45 + (2i \mp 1)0.25$, (class A_i), $i = 1, 2, 3$, and the horizontal branch, $[\text{Fe}/\text{H}] = -1.6 \mp 0.2$, are also plotted (dashed). M13 sample stars directly shift from the main sequence, $[\text{Fe}/\text{H}] = [\text{O}/\text{H}] - 0.45 \mp 0.25$, (class A_0), to the horizontal branch. For further details refer to the text.

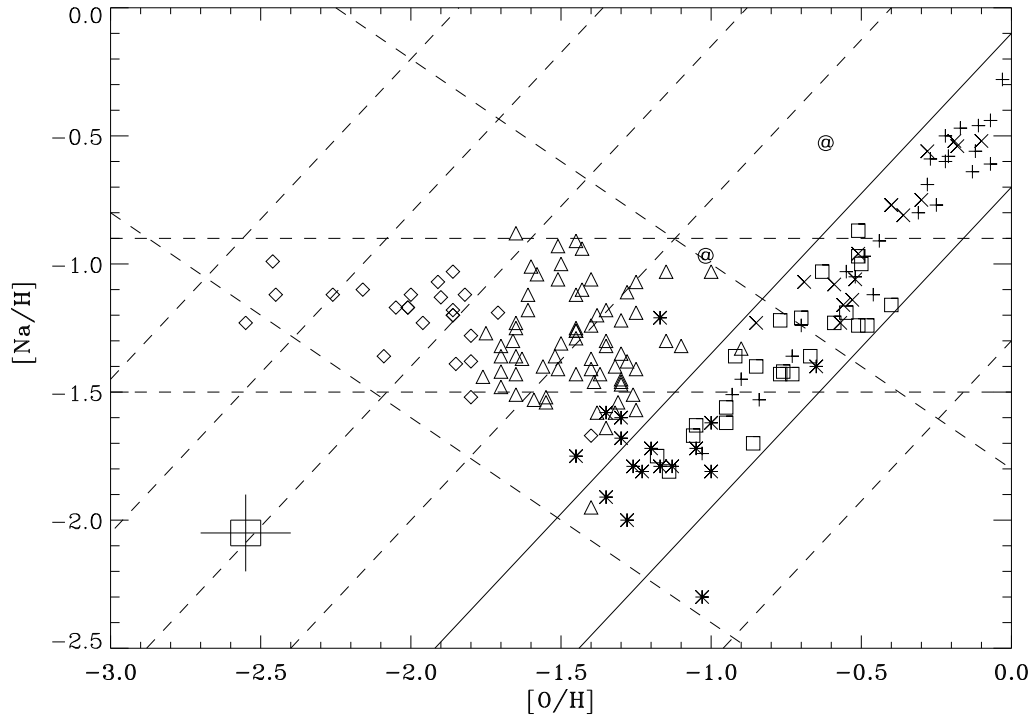


Figure 4: Zoom of Fig. 2, bottom right panel, where the parallel sequences, $[\text{Na}/\text{H}] = 1.25 [\text{O}/\text{H}] - 0.40 + (2i \mp 1)0.30$, (class A_i), $i = -1, 1, 2, 3, 4$, the horizontal branch, $[\text{Na}/\text{H}] = -1.2 \mp 0.3$, and the O-Na anticorrelation, $[\text{Na}/\text{H}] = -0.8 [\text{O}/\text{H}] - 2.5 \mp 0.7$, are also plotted (dashed). M13 sample stars shift from the main sequence, $[\text{Na}/\text{H}] = 1.25 [\text{O}/\text{H}] - 0.40 \mp 0.30$, (class A_0), to the horizontal branch via the parallel sequence, $[\text{Na}/\text{H}] = 1.25 [\text{O}/\text{H}] + 0.20 \mp 0.30$. For further details refer to the text.

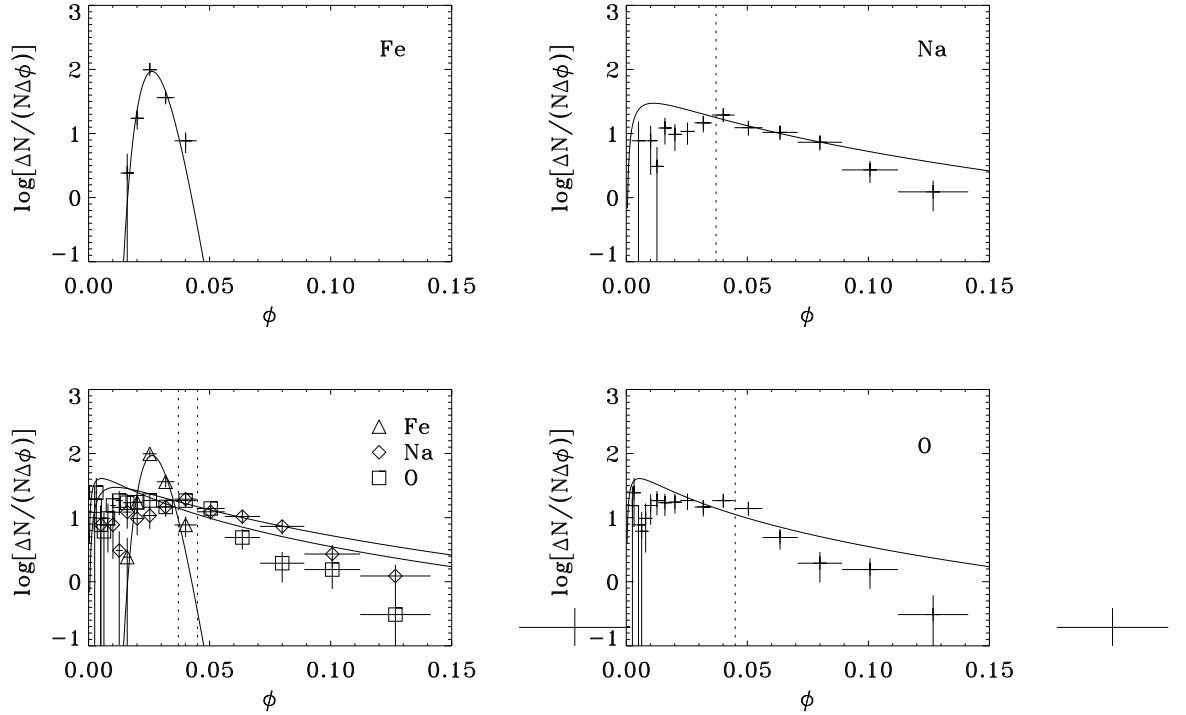


Figure 5: M13 empirical differential abundance distribution deduced from the JP12 sample related to Fe (top left panel), Na (top right panel), O (bottom right panel), all together (bottom left panel). The point out of scale corresponds to oxygen abundance within a single star. The theoretical differential abundance distribution due to cosmic scatter obeying a Gaussian distribution where $(x^*, \sigma_x) = (\langle [Q/H] \rangle, \sigma_{[Q/H]})$, is also plotted on each panel for Fe, Na, O, when appropriate. The dotted vertical lines mark $\phi_O = 0.045$ or $[O/H] = -1.35$ and $\phi_{Na} = 0.037$ or $[Na/H] = -1.45$, when appropriate. For further details refer to the text.

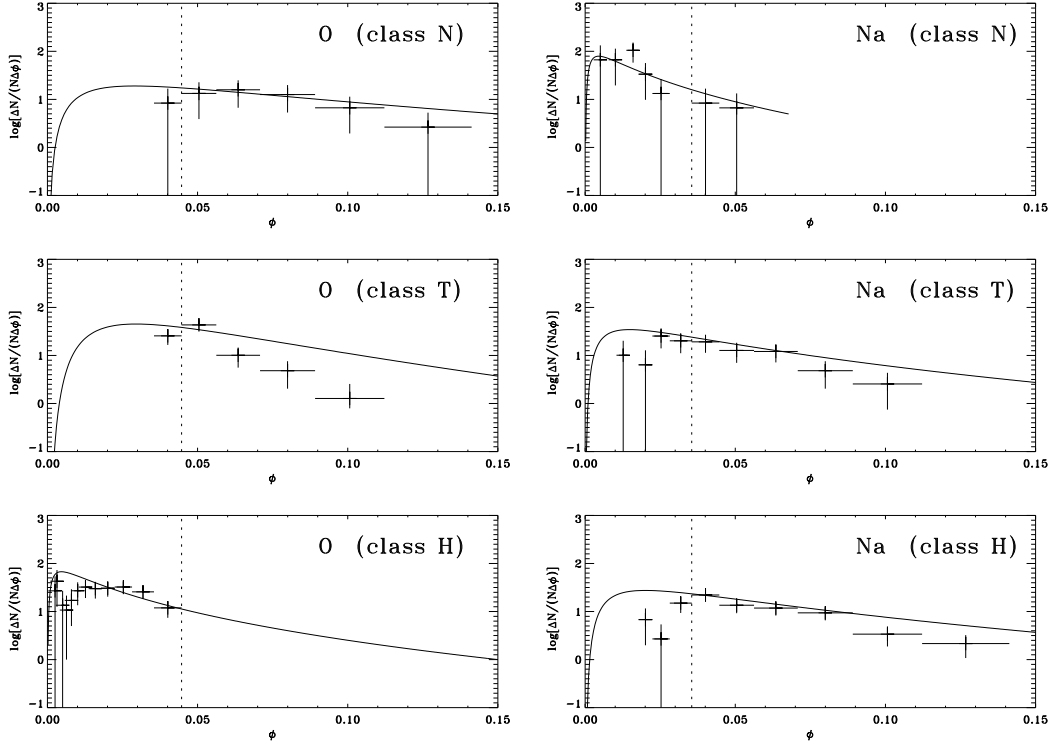


Figure 6: M13 empirical differential abundance distribution deduced from the JP12 sample for stars belonging to class N ($N = 13$), T ($N = 34$), H ($N = 64$), related to O (left panels) and Na (right panels). The theoretical differential distribution due to cosmic scatter obeying a Gaussian distribution where $(x^*, \sigma_x) = (\langle [Q/H] \rangle, \sigma_{[Q/H]})$, is also plotted on each panel for O, Na, when appropriate. The dotted vertical lines mark $\phi_O = 0.045$ or $[O/H] = -1.35$ and $\phi_{Na} = 0.035$ or $[Na/H] = -1.45$, when appropriate. For further details refer to the text.

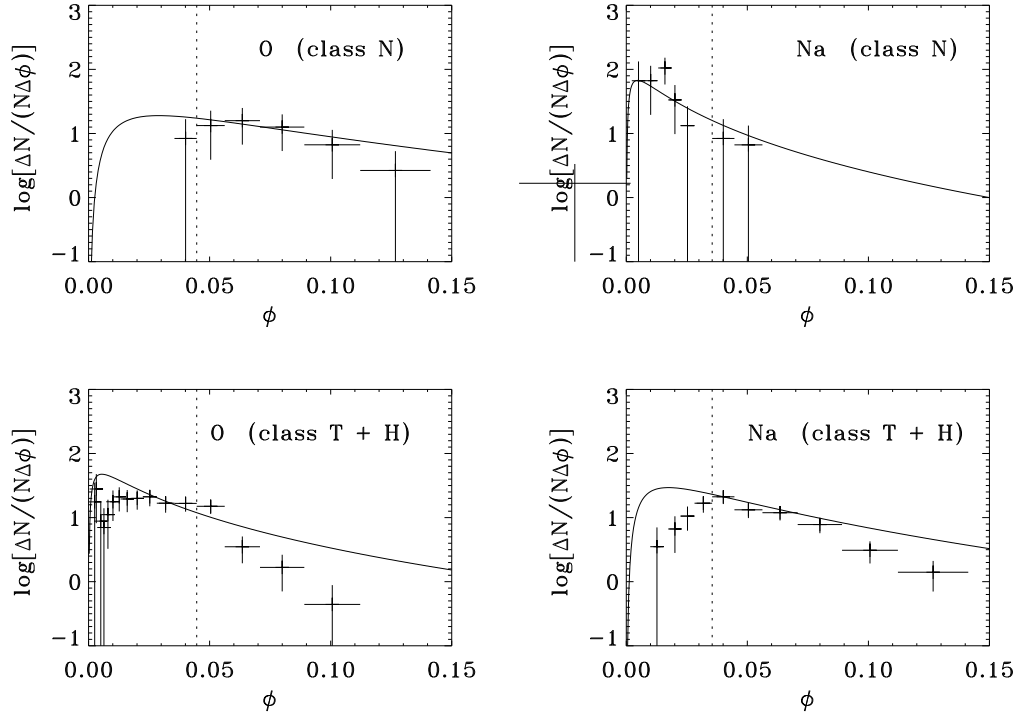


Figure 7: M13 empirical differential abundance distribution deduced from the JP12 sample for stars belonging to class N ($N = 13$), T+H ($N = 98$), related to O (left panels) and Na (right panels). The point out of scale corresponds to oxygen abundance within a single star. Other captions as in Fig. 6.

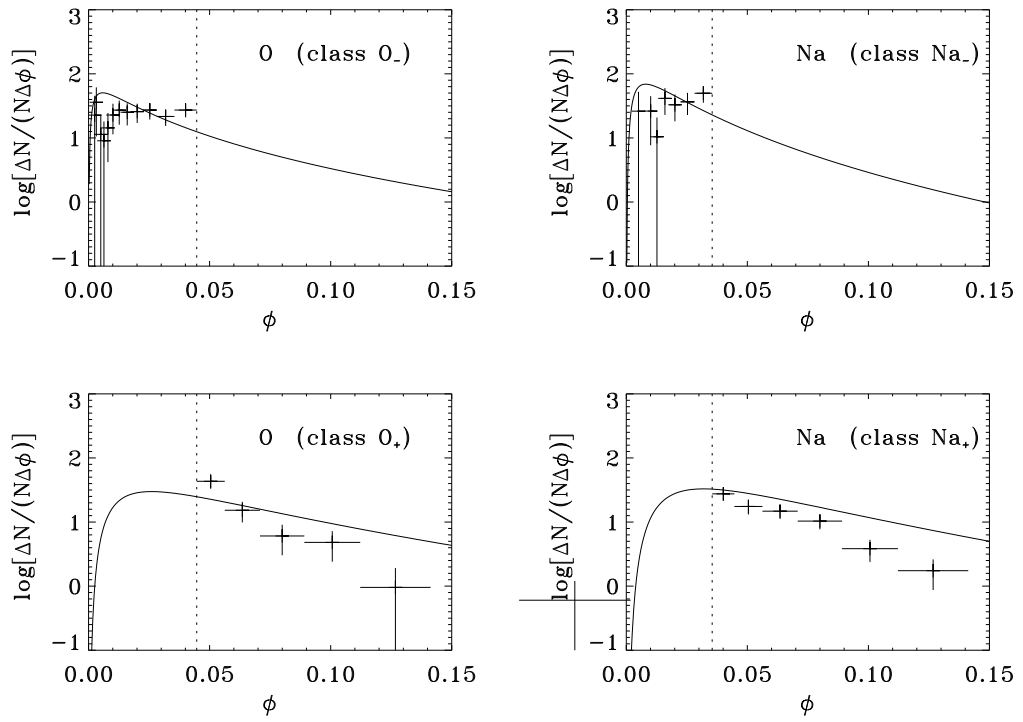


Figure 8: M13 empirical differential abundance distribution deduced from the JP12 sample for stars belonging to class O_- ($N = 76$), O_+ ($N = 36$), Na_- ($N = 33$), Na_+ ($N = 79$). Other captions as in Fig. 7.

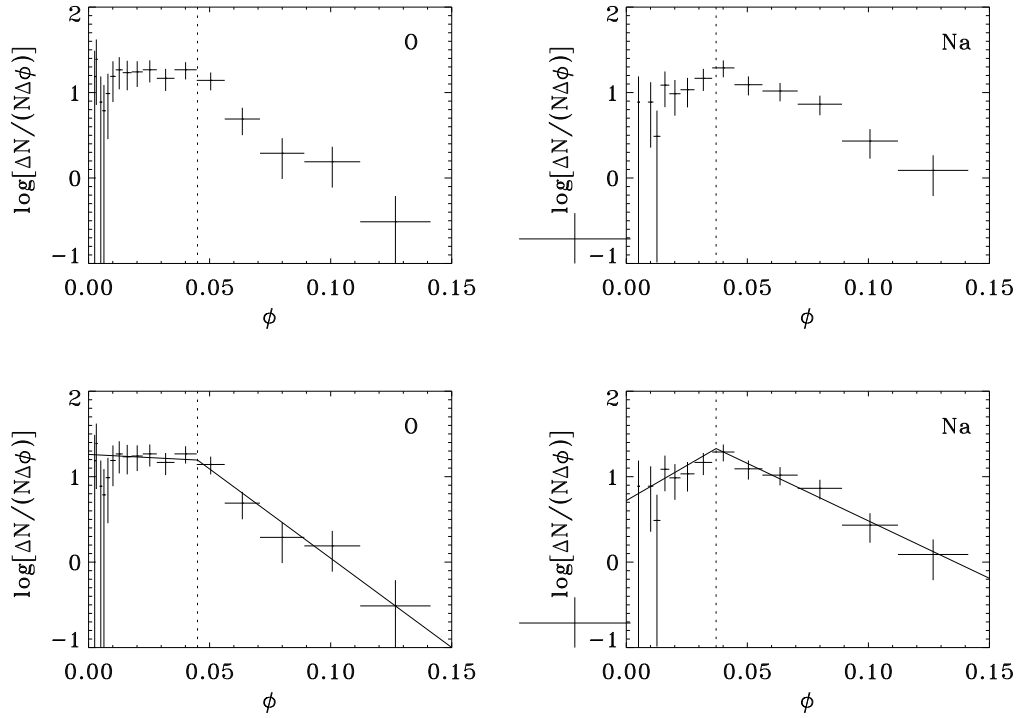


Figure 9: Regression lines to the empirical differential oxygen (top left) and sodium (top right) abundance distributions listed in Table 3 with regard to stages (from the left to the right) AF and CE. Bins containing a single star are not used for the regression. The abscissa of the intersection point of regression lines is marked by a dashed vertical line. Other captions as in Fig. 5. For further details refer to the text.